The 9th European Congress on Computational Methods in Applied Sciences and Engineering
ECCOMAS Congress 2024
3–7 June 2024, Lisboa, Portugal

VALIDATION OF A NUMERICAL MODEL OF SEISMIC NEWTONIAN NOISE FOR THE EINSTEIN TELESCOPE

PIETER REUMERS, STIJN FRANÇOIS AND GEERT DEGRANDE

KU Leuven, Department of Civil Engineering, Structural Mechanics Section
Kasteelpark Arenberg 40, B-3001 Leuven, Belgium
e-mail: pieter.reumers@kuleuven.be

Key words: Newtonian noise, seismic wave propagation, Einstein Telescope

1 INTRODUCTION

The Einstein Telescope (ET) is a third-generation gravitational wave (GW) detector that is planned to be constructed in the coming decade. It consists of an underground, triangular laser interferometer and is designed to observe GWs – ripples in the 4D space-time continuum – due to e.g. binary black hole or binary neutron star mergers. The mirrors of the laser interferometer are installed in suspension towers placed inside large cavities at the corner points of the interferometer.

To observe GWs caused by mergers at larger distance or with a larger mass, the sensitivity and operating frequency range (above 10 Hz) of current second-generation GW observatories is insufficient. To improve the sensitivity by one order of magnitude and lower the operating frequency to 3 Hz, the ET is preferably constructed underground in a seismically quiet region [1] so that disturbance by anthropogenic vibration sources such as road and railway traffic or wind turbines is maximally reduced.

Seismic Newtonian noise (NN) dominates at low frequencies: seismic waves propagating in the soil generate density fluctuations which result in gravitational attraction and corresponding motion of the mirrors of the laser interferometer. Since these gravitational forces cannot be shielded, the only remedy is to estimate seismic NN from seismic measurements through wavefield reconstruction and subtract it from the interferometer data [2].

This paper presents a numerical model in which the soil domain surrounding a cavity is discretized with finite elements. Gaussian quadrature is used to numerically evaluate the volume integrals quantifying the NN. The model accounts for wave scattering by the cavity and is validated using analytical expressions for plane waves propagating in a homogeneous fullspace [3]. The influence of wave scattering and the size of the cavity around the mirror on the NN is studied.

2 THEORETICAL BACKGROUND

Seismic NN is the undesired motion (acceleration) caused by gravitational attraction of the mirror of the laser interferometer due to density fluctuations in the soil. These fluctuations are induced by seismic waves with a compressional component. Shear waves do not generate NN, unless they impinge on layer interfaces or free surfaces.

2.1 Governing equations

The gravitational force F between two point masses M and m is determined by the gravitational constant $G \approx 6.6743 \times 10^{-11}\,\mathrm{m^3/kg/s^2}$ and their spacing r:

$$F \;=\; G\frac{Mm}{r^2} \tag{1}$$

The gravitational potential $\phi(r)$ [Nm/kg] is defined as the work per unit mass required to move the mass m from infinity (where $\phi = 0$) to a distance r from the mass M:

$$\phi(r) \;=\; \frac{1}{m}\int_{+\infty}^{r} G\frac{Mm}{x^2}\,\mathrm{d}x \;=\; -\,G\frac{M}{r} \tag{2}$$

The value of $\phi(r)$ is always negative, as work is required to pull objects away from large masses such as the Earth. When a volume V with density $\rho(\mathbf{x})$ is considered instead of the point mass M, the gravitational potential $\phi(\mathbf{x}_0)$ at a position $\mathbf{x}_0$ is expressed as follows:

$$\phi(\mathbf{x}_0) \;=\; -\,G\int_V \frac{\rho(\mathbf{x})}{|\mathbf{x}-\mathbf{x}_0|}\,\mathrm{d}V \tag{3}$$

The gravitational acceleration $\mathbf{a}(\mathbf{x}_0)$ [$\mathrm{m/s^2}$], or gravitational force per unit mass, is computed as the negative gradient of the gravitational potential $\phi(\mathbf{x}_0)$:

$$\mathbf{a}(\mathbf{x}_0) \;=\; -\,\nabla_0\phi(\mathbf{x}_0) \;=\; G\int_V \rho(\mathbf{x})\boldsymbol{\chi}(\mathbf{x},\mathbf{x}_0)\,\mathrm{d}V \tag{4}$$

where ∇_0 denotes the gradient operator with respect to $\mathbf{x}_0$ and $\boldsymbol{\chi}(\mathbf{x},\mathbf{x}_0)$ is defined as:

$$\boldsymbol{\chi}(\mathbf{x},\mathbf{x}_0) \;=\; \frac{\mathbf{x}-\mathbf{x}_0}{|\mathbf{x}-\mathbf{x}_0|^3} \tag{5}$$

The acceleration $\mathbf{a}(\mathbf{x}_0)$ is positive towards the elementary volume $\mathrm{d}V(\mathbf{x})$.

Consider now a seismic displacement field $\hat{\mathbf{u}}(\mathbf{x},\omega)$ [m/Hz] inside a soil volume V. The propagation of seismic waves generates density fluctuations $\delta\hat{\rho}(\mathbf{x},\omega)$ [$\mathrm{kg/m^3/Hz}$], which are determined from the conservation of mass:

$$\delta\hat{\rho}(\mathbf{x},\omega) \;=\; -\,\nabla\cdot(\rho(\mathbf{x})\hat{\mathbf{u}}(\mathbf{x},\omega)) \tag{6}$$

The hat above a variable denotes its representation in the frequency domain; the explicit dependence on the frequency ω is omitted from the notation in the remainder of this paper. The divergence operator in equation (6) can be further elaborated using the product rule:

$$\delta\hat{\rho}(\mathbf{x}) \;=\; -\,\rho(\mathbf{x})\nabla\cdot\hat{\mathbf{u}}(\mathbf{x}) - \hat{\mathbf{u}}(\mathbf{x})\cdot\nabla\rho(\mathbf{x}) \tag{7}$$

In a homogeneous medium where $\nabla\rho(\mathbf{x}) = 0$, shear waves do not generate NN since the divergence of the displacement field $\nabla\cdot\hat{\mathbf{u}}(\mathbf{x})$ is equal to zero. However, in heterogeneous soils or near free surfaces, the gradient of the density $\nabla\rho(\mathbf{x})$ is no longer zero, and shear waves also contribute to the NN.

Assuming that a mirror of the laser interferometer can be represented as a point mass at the position $\mathbf{x}_0$, the perturbation $\delta\hat{\phi}(\mathbf{x}_0)$ [Nm/kg/Hz] in its gravitational potential due to density fluctuations $\delta\hat{\rho}(\mathbf{x})$ inside the soil volume V is given by:

$$\delta\hat{\phi}(\mathbf{x}_0) \;=\; -G\int_V \frac{\delta\hat{\rho}(\mathbf{x})}{|\mathbf{x}-\mathbf{x}_0|}\,\mathrm{d}V(\mathbf{x}) \tag{8}$$

Substituting equation (6) into equation (8) yields:

$$\delta\hat{\phi}(\mathbf{x}_0) \;=\; G\int_V \frac{\nabla\cdot(\rho(\mathbf{x})\hat{\mathbf{u}}(\mathbf{x}))}{|\mathbf{x}-\mathbf{x}_0|}\,\mathrm{d}V \tag{9}$$

Integrating by parts, assuming an infinitely large volume V, gives:

$$\delta\hat{\phi}(\mathbf{x}_0) \;=\; -G\int_V \rho(\mathbf{x})\hat{\mathbf{u}}(\mathbf{x})\cdot\nabla\frac{1}{|\mathbf{x}-\mathbf{x}_0|}\,\mathrm{d}V \;=\; G\int_V \rho(\mathbf{x})\hat{\mathbf{u}}(\mathbf{x})\cdot\boldsymbol{\chi}(\mathbf{x},\mathbf{x}_0)\,\mathrm{d}V(\mathbf{x}) \tag{10}$$

The corresponding perturbation $\delta\hat{\mathbf{a}}(\mathbf{x}_0)$ [m/s^2/Hz] in the gravitational acceleration is given by equation (4):

$$\begin{aligned}
\delta\hat{\mathbf{a}}(\mathbf{x}_0) \;&=\; -\nabla_0\delta\hat{\phi}(\mathbf{x}_0)\\
&=\; -G\int_V \rho(\mathbf{x})\nabla_0\left(\hat{\mathbf{u}}(\mathbf{x})\cdot\boldsymbol{\chi}(\mathbf{x},\mathbf{x}_0)\right)\,\mathrm{d}V\\
&=\; -G\int_V \rho(\mathbf{x})\left(\hat{\mathbf{u}}(\mathbf{x})\cdot\nabla_0\right)\boldsymbol{\chi}(\mathbf{x},\mathbf{x}_0)\,\mathrm{d}V - G\int_V \rho(\mathbf{x})\hat{\mathbf{u}}(\mathbf{x})\times\left(\nabla_0\times\boldsymbol{\chi}(\mathbf{x},\mathbf{x}_0)\right)\,\mathrm{d}V
\end{aligned} \tag{11}$$

where $\times$ denotes the cross product of two vectors. In equation (11), the second term vanishes because the curl $\nabla_0\times\boldsymbol{\chi}(\mathbf{x},\mathbf{x}_0)$ is equal to zero. Further elaboration gives:

$$\delta\hat{\mathbf{a}}(\mathbf{x}_0) \;=\; -G\int_V \rho(\mathbf{x})\left(\hat{\mathbf{u}}(\mathbf{x})\cdot\nabla_0\right)\boldsymbol{\chi}(\mathbf{x},\mathbf{x}_0)\,\mathrm{d}V \;=\; -G\int_V \rho(\mathbf{x})\nabla_0\boldsymbol{\chi}(\mathbf{x},\mathbf{x}_0)\cdot\hat{\mathbf{u}}(\mathbf{x})\,\mathrm{d}V \tag{12}$$

This expression yields the total NN $\delta\hat{\mathbf{a}}(\mathbf{x}_0)$ at the mirror position $\mathbf{x}_0$ due to the seismic displacement field $\hat{\mathbf{u}}(\mathbf{x})$. By discretizing the soil volume V with finite elements, the volume integral can be evaluated numerically using Gaussian quadrature. This is the subject of subsection 3.2.

2.2 Bulk and surface contributions

Consider the heterogeneous soil volume V consisting of two materials with density ρ_1 (volume V_1) and ρ_2 (volume V_2) shown in figure 1. The interface between V_1 and V_2 is described by the plane $S(\mathbf{x}) = 0$, with $S(\mathbf{x})$ normalized such that $\nabla S(\mathbf{x})$ is equal to the unit normal vector $\mathbf{n}_1(\mathbf{x})$ pointing outwards of V_1. The density $\rho(\mathbf{x})$ inside V is then expressed using the Heaviside function $H(x)$:

$$\rho(\mathbf{x}) \;=\; \rho_1 + \Delta\rho H(S(\mathbf{x})) \tag{13}$$

where $\Delta\rho = \rho_2 - \rho_1$. Substituting this expression for $\rho(\mathbf{x})$ into equation (9) yields:

$$\delta\hat{\phi}(\mathbf{x}_0) \;=\; G\int_V \frac{\nabla\cdot[(\rho_1 + \Delta\rho H(S(\mathbf{x})))\hat{\mathbf{u}}(\mathbf{x})]}{|\mathbf{x}-\mathbf{x}_0|}\,\mathrm{d}V \tag{14}$$

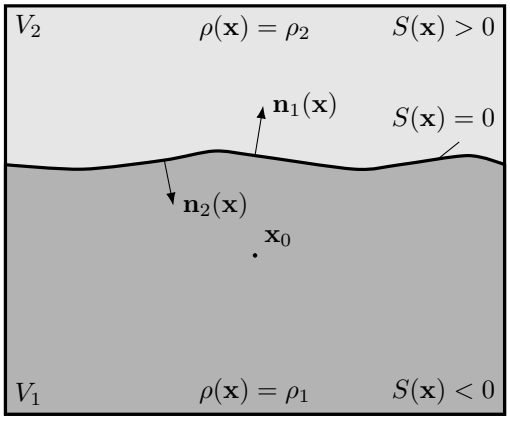

Figure 1: Heterogeneous soil mass V consisting of two materials with densities ρ_1 and ρ_2, separated by the interface $S(\mathbf{x})$. The unit outward normal vector on V_1 equals $\mathbf{n}_1(\mathbf{x}) = -\mathbf{n}_2(\mathbf{x})$.

Application of the product rule results in:

$$\delta\hat{\phi}(\mathbf{x}_0) \;=\; G\int_V \frac{(\rho_1 + \Delta\rho H(S(\mathbf{x}))\,(\nabla\cdot\hat{\mathbf{u}}(\mathbf{x}))}{|\mathbf{x}-\mathbf{x}_0|}\,\mathrm{d}V + G\int_V \frac{\hat{\mathbf{u}}(\mathbf{x})\cdot[\Delta\rho\nabla H(S(\mathbf{x}))]}{|\mathbf{x}-\mathbf{x}_0|}\,\mathrm{d}V \tag{15}$$

The gradient of the Heaviside function in the second term is elaborated using the chain rule:

$$\nabla H(S(\mathbf{x})) \;=\; \delta(S(\mathbf{x}))\nabla S(\mathbf{x}) \;=\; \delta(S(\mathbf{x}))\mathbf{n}_1(\mathbf{x}) \tag{16}$$

where $\delta(x)$ is the Dirac delta function. The Heaviside function in the first term of equation (15) results in the sum of volume integrals over V_1 and V_2, while the second term, after substituting equation (16), becomes a surface integral over $S(\mathbf{x})$ due to the presence of the Dirac delta function:

$$\delta\hat{\phi}(\mathbf{x}_0) \;=\; G\rho_1\int_{V_1}\frac{\nabla\cdot\hat{\mathbf{u}}(\mathbf{x})}{|\mathbf{x}-\mathbf{x}_0|}\,\mathrm{d}V + G\rho_2\int_{V_2}\frac{\nabla\cdot\hat{\mathbf{u}}(\mathbf{x})}{|\mathbf{x}-\mathbf{x}_0|}\,\mathrm{d}V + G\Delta\rho\int_S\frac{\hat{\mathbf{u}}(\mathbf{x})\cdot\mathbf{n}_1(\mathbf{x})}{|\mathbf{x}-\mathbf{x}_0|}\,\mathrm{d}S \tag{17}$$

The first two terms can be interpreted as bulk contributions of V_1 and V_2, respectively. The third term is the surface contribution due to the density change $\Delta\rho$ at the interface S, and can be elaborated as:

$$G\Delta\rho\int_S\frac{\hat{\mathbf{u}}(\mathbf{x})\cdot\mathbf{n}_1(\mathbf{x})}{|\mathbf{x}-\mathbf{x}_0|}\,\mathrm{d}S \;=\; -G\rho_1\int_S\frac{\hat{\mathbf{u}}(\mathbf{x})\cdot\mathbf{n}_1(\mathbf{x})}{|\mathbf{x}-\mathbf{x}_0|}\,\mathrm{d}S - G\rho_2\int_S\frac{\hat{\mathbf{u}}(\mathbf{x})\cdot\mathbf{n}_2(\mathbf{x})}{|\mathbf{x}-\mathbf{x}_0|}\,\mathrm{d}S \tag{18}$$

where $\mathbf{n}_2(\mathbf{x}) = -\mathbf{n}_1(\mathbf{x})$ is the unit normal vector pointing outwards of V_2. By taking the negative gradient $-\nabla_0\delta\hat{\phi}(\mathbf{x}_0)$ of equation (17), the bulk and surface contributions to the NN $\delta\hat{\mathbf{a}}(\mathbf{x}_0)$ are obtained:

$$\begin{aligned}\delta\hat{\mathbf{a}}(\mathbf{x}_0) \;&= G\rho_1\int_{V_1}(\nabla\cdot\hat{\mathbf{u}}(\mathbf{x}))\,\boldsymbol{\chi}(\mathbf{x},\mathbf{x}_0)\,\mathrm{d}V - G\rho_1\int_S(\hat{\mathbf{u}}(\mathbf{x})\cdot\mathbf{n}_1(\mathbf{x}))\,\boldsymbol{\chi}(\mathbf{x},\mathbf{x}_0)\,\mathrm{d}S\\ &+ G\rho_2\int_{V_2}(\nabla\cdot\hat{\mathbf{u}}(\mathbf{x}))\,\boldsymbol{\chi}(\mathbf{x},\mathbf{x}_0)\,\mathrm{d}V - G\rho_2\int_S(\hat{\mathbf{u}}(\mathbf{x})\cdot\mathbf{n}_2(\mathbf{x}))\,\boldsymbol{\chi}(\mathbf{x},\mathbf{x}_0)\,\mathrm{d}S\end{aligned} \tag{19}$$

In the particular case that $\rho_1 = \rho_2$, the surface contributions cancel and the total NN is given as the sum of both bulk contributions.

3 NUMERICAL MODEL

We compute NN using a two-step procedure. First, we determine an incoming seismic wave field $\hat{\mathbf{u}}^{\text{inc}}(\mathbf{x})$ obtained either analytically (e.g. plane waves), as the solution of the elastodynamic wave equations for a horizontally layered medium [4], or with commercial software such as COMSOL or SPECFEM3D. Wave scattering by the cavity is taken into account using the subdomain formulation proposed by Bielak et al. [5]. The total wave field $\hat{\mathbf{u}}(\mathbf{x})$ is then equal to the sum of the incoming wave field $\hat{\mathbf{u}}^{\text{inc}}(\mathbf{x})$ and the scattered wave field $\hat{\mathbf{u}}^{\text{sc}}(\mathbf{x})$. Next, the NN due to the wave field $\hat{\mathbf{u}}(\mathbf{x})$ is computed in a post-processing step on a finite element (FE) mesh using Gaussian quadrature.

We first discuss the computation of the scattered wave field $\hat{\mathbf{u}}^{\text{sc}}(\mathbf{x})$. Subsequently, the FE discretization of equation (12) is presented to predict NN.

3.1 Computation of the scattered wave field

To compute the scattered wave field $\hat{\mathbf{u}}^{\text{sc}}(\mathbf{x})$ due to an incoming wave field $\hat{\mathbf{u}}^{\text{inc}}(\mathbf{x})$ impinging on a cavity, we use the subdomain formulation by Bielak et al. [5]. Figure 2 shows an overview of the involved subdomains; for simplicity, the geometry is shown in 2D, but the formulation is identical in 3D.

In figure 2a, the volume V_{i} contains the cavity and part of the soil surrounding it. The volume V_{e} consists of the soil outside V_{i}. The soil displacements are partitioned using the subscripts i, e and b, denoting the displacements inside V_{i}, inside V_{e}, and on the boundary Σ between V_{i} and V_{e}, respectively. The volumes V_{i} and V_{e} are discretized using FE, and their dynamic stiffness matrices $\mathbf{D}^{\text{i}} = \mathbf{K}^{\text{i}} - \omega^2\mathbf{M}^{\text{i}}$ and $\mathbf{D}^{\text{e}} = \mathbf{K}^{\text{e}} - \omega^2\mathbf{M}^{\text{e}}$ are assembled. Hysteretic damping is assumed, resulting in complex-valued stiffness matrices $\mathbf{K}^{\text{i}}$ and $\mathbf{K}^{\text{e}}$. The equations of motion for the problem in figure 2a are:

$$\begin{bmatrix} \mathbf{D}^{\text{i}}_{\text{ii}} & \mathbf{D}^{\text{i}}_{\text{ib}} & \mathbf{0} \\ \mathbf{D}^{\text{i}}_{\text{bi}} & \mathbf{D}^{\text{i}}_{\text{bb}} + \mathbf{D}^{\text{e}}_{\text{bb}} & \mathbf{D}^{\text{e}}_{\text{be}} \\ \mathbf{0} & \mathbf{D}^{\text{e}}_{\text{eb}} & \mathbf{D}^{\text{e}}_{\text{ee}} \end{bmatrix} \begin{Bmatrix} \hat{\mathbf{u}}_{\text{i}} \\ \hat{\mathbf{u}}_{\text{b}} \\ \hat{\mathbf{u}}_{\text{e}} \end{Bmatrix} = \begin{Bmatrix} \mathbf{0} \\ \mathbf{0} \\ \hat{\mathbf{f}}_{\text{e}} \end{Bmatrix} \tag{20}$$

where $\hat{\mathbf{f}}_{\text{e}}$ is a set of external forces that induce the incoming displacement field $\hat{\mathbf{u}}^{\text{inc}}$. The total displacement field $\hat{\mathbf{u}}_{\text{e}}$ in the exterior volume V_{e} can be written as a superposition of the incoming displacement field $\hat{\mathbf{u}}^{\text{inc}}_{\text{e}}$ (in the absence of the cavity) and the scattered displacement field $\hat{\mathbf{u}}^{\text{sc}}_{\text{e}}$:

$$\hat{\mathbf{u}}_{\text{e}} = \hat{\mathbf{u}}^{\text{inc}}_{\text{e}} + \hat{\mathbf{u}}^{\text{sc}}_{\text{e}} \tag{21}$$

Substituting equation (21) into the system of equations (20) yields:

$$\begin{bmatrix} \mathbf{D}^{\text{i}}_{\text{ii}} & \mathbf{D}^{\text{i}}_{\text{ib}} & \mathbf{0} \\ \mathbf{D}^{\text{i}}_{\text{bi}} & \mathbf{D}^{\text{i}}_{\text{bb}} + \mathbf{D}^{\text{e}}_{\text{bb}} & \mathbf{D}^{\text{e}}_{\text{be}} \\ \mathbf{0} & \mathbf{D}^{\text{e}}_{\text{eb}} & \mathbf{D}^{\text{e}}_{\text{ee}} \end{bmatrix} \begin{Bmatrix} \hat{\mathbf{u}}_{\text{i}} \\ \hat{\mathbf{u}}_{\text{b}} \\ \hat{\mathbf{u}}^{\text{sc}}_{\text{e}} \end{Bmatrix} = \begin{Bmatrix} \mathbf{0} \\ -\mathbf{D}^{\text{e}}_{\text{be}}\hat{\mathbf{u}}^{\text{inc}}_{\text{e}} \\ \hat{\mathbf{f}}_{\text{e}} - \mathbf{D}^{\text{e}}_{\text{ee}}\hat{\mathbf{u}}^{\text{inc}}_{\text{e}} \end{Bmatrix} \tag{22}$$

Consider now a second problem in figure 2b, where the volume V_{i} is replaced by $V_{\text{i}'}$ in which the cavity is removed and the soil heterogeneity is simplified, so that the incoming wave field $\hat{\mathbf{u}}^{\text{inc}}(\mathbf{x})$ can easily be computed. The exterior volume V_{e} is identical as in figure 2a. The equations of

motion for this problem are:

$$\begin{bmatrix} \mathbf{D}^{\mathrm{i}'}_{\mathrm{ii}} & \mathbf{D}^{\mathrm{i}'}_{\mathrm{ib}} & \mathbf{0} \\ \mathbf{D}^{\mathrm{i}'}_{\mathrm{bi}} & \mathbf{D}^{\mathrm{i}'}_{\mathrm{bb}} + \mathbf{D}^{\mathrm{e}}_{\mathrm{bb}} & \mathbf{D}^{\mathrm{e}}_{\mathrm{be}} \\ \mathbf{0} & \mathbf{D}^{\mathrm{e}}_{\mathrm{eb}} & \mathbf{D}^{\mathrm{e}}_{\mathrm{ee}} \end{bmatrix} \begin{Bmatrix} \hat{\mathbf{u}}^{\mathrm{inc}}_{\mathrm{i}} \\ \hat{\mathbf{u}}^{\mathrm{inc}}_{\mathrm{b}} \\ \hat{\mathbf{u}}^{\mathrm{inc}}_{\mathrm{e}} \end{Bmatrix} = \begin{Bmatrix} \mathbf{0} \\ \mathbf{0} \\ \hat{\mathbf{f}}_{\mathrm{e}} \end{Bmatrix} \tag{23}$$

where $\mathbf{D}^{\mathrm{i}'}$ denotes the dynamic stiffness matrix of the volume $V_{\mathrm{i}'}$. Since the incoming displacements $\hat{\mathbf{u}}^{\mathrm{inc}}_{\mathrm{b}}$ and $\hat{\mathbf{u}}^{\mathrm{inc}}_{\mathrm{e}}$ are known, the external force vector can be computed from the bottom row in equation (23):

$$\hat{\mathbf{f}}_{\mathrm{e}} = \mathbf{D}^{\mathrm{e}}_{\mathrm{eb}} \hat{\mathbf{u}}^{\mathrm{inc}}_{\mathrm{b}} + \mathbf{D}^{\mathrm{e}}_{\mathrm{ee}} \hat{\mathbf{u}}^{\mathrm{inc}}_{\mathrm{e}} \tag{24}$$

Substituting equation (24) into the system of equations (22) yields:

$$\begin{bmatrix} \mathbf{D}^{\mathrm{i}}_{\mathrm{ii}} & \mathbf{D}^{\mathrm{i}}_{\mathrm{ib}} & \mathbf{0} \\ \mathbf{D}^{\mathrm{i}}_{\mathrm{bi}} & \mathbf{D}^{\mathrm{i}}_{\mathrm{bb}} + \mathbf{D}^{\mathrm{e}}_{\mathrm{bb}} & \mathbf{D}^{\mathrm{e}}_{\mathrm{be}} \\ \mathbf{0} & \mathbf{D}^{\mathrm{e}}_{\mathrm{eb}} & \mathbf{D}^{\mathrm{e}}_{\mathrm{ee}} \end{bmatrix} \begin{Bmatrix} \hat{\mathbf{u}}_{\mathrm{i}} \\ \hat{\mathbf{u}}_{\mathrm{b}} \\ \hat{\mathbf{u}}^{\mathrm{sc}}_{\mathrm{e}} \end{Bmatrix} = \begin{Bmatrix} \mathbf{0} \\ -\mathbf{D}^{\mathrm{e}}_{\mathrm{be}} \hat{\mathbf{u}}^{\mathrm{inc}}_{\mathrm{e}} \\ +\mathbf{D}^{\mathrm{e}}_{\mathrm{eb}} \hat{\mathbf{u}}^{\mathrm{inc}}_{\mathrm{b}} \end{Bmatrix} \tag{25}$$

which can be solved for the total displacement fields $\hat{\mathbf{u}}_{\mathrm{i}}$ and $\hat{\mathbf{u}}_{\mathrm{b}}$, and the scattered displacement field $\hat{\mathbf{u}}^{\mathrm{sc}}_{\mathrm{e}}$.

The force vector on the right hand side of equation (25) depends on the known incoming displacement field and the submatrices $\mathbf{D}^{\mathrm{e}}_{\mathrm{be}}$ and $\mathbf{D}^{\mathrm{e}}_{\mathrm{eb}}$ of the dynamic stiffness matrix $\mathbf{D}^{\mathrm{e}}$. In order to compute the latter, the external volume V_{e} needs to be meshed with at least one layer of elements next to the boundary Σ. Any additional elements are not connected to Σ and, hence, do not contribute to $\mathbf{D}^{\mathrm{e}}_{\mathrm{be}}$ and $\mathbf{D}^{\mathrm{e}}_{\mathrm{eb}}$, but only to $\mathbf{D}^{\mathrm{e}}_{\mathrm{ee}}$. Furthermore, a perfectly matched layer (PML) [6, 7] is used at the boundary Γ_{e} (figure 2) to absorb the out-going scattered waves.

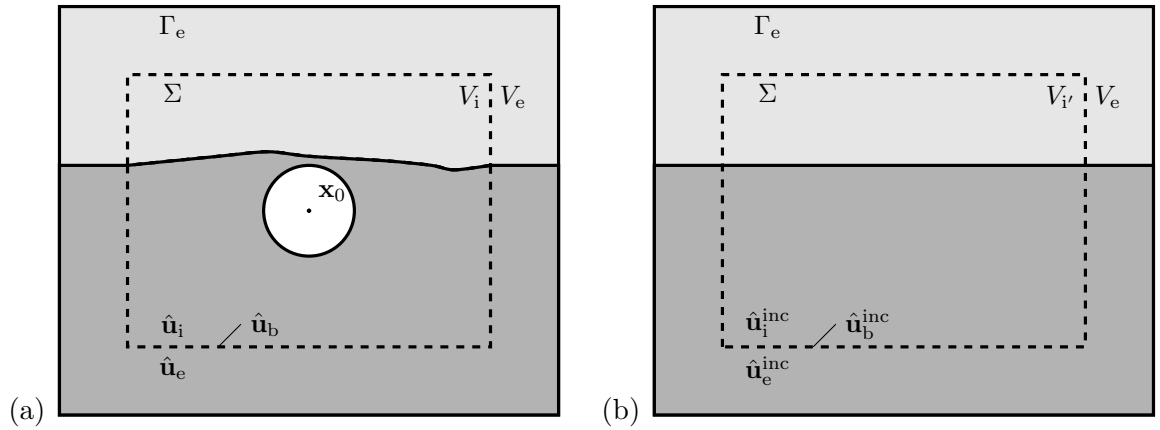

Figure 2: Subdomain formulation proposed by Bielak et al. [5] to compute the scattered wave field. Problem involving (a) the total displacement field $\hat{\mathbf{u}}$ and (b) the incoming displacement field $\hat{\mathbf{u}}^{\mathrm{inc}}$.

3.2 Computation of NN on an FE mesh using Gaussian quadrature

In order to evaluate the volume integral in equation (12), the volume V is discretized into n^e finite elements (FE) with volume V^e and constant density ρ^e, resulting in the following sum:

$$\delta\hat{\mathbf{a}}(\mathbf{x}_0) = \sum_{e=1}^{n^e} G \int_{V^e} \rho^e \nabla\boldsymbol{\chi}(\mathbf{x}, \mathbf{x}_0) \cdot \hat{\mathbf{u}}^e(\mathbf{x}) \, \mathrm{d}V^e \tag{26}$$

where $\hat{\mathbf{u}}^e(\mathbf{x})$ are the element displacements. The equality $\nabla_0\boldsymbol{\chi}(\mathbf{x},\mathbf{x}_0) = -\nabla\boldsymbol{\chi}(\mathbf{x},\mathbf{x}_0)$ is used in equation (26). Within each FE, an isoparametric transformation is employed to transform the global coordinate $\mathbf{x} = (x_1, x_2, x_3)$ to a local (element) coordinate $\boldsymbol{\xi} = (\xi_1, \xi_2, \xi_3)$ using shape functions $N_k^e(\boldsymbol{\xi})$:

$$\mathbf{x}(\boldsymbol{\xi}) \;=\; \sum_{k=1}^{n} \begin{bmatrix} N_k^e(\boldsymbol{\xi}) & 0 & 0 \\ 0 & N_k^e(\boldsymbol{\xi}) & 0 \\ 0 & 0 & N_k^e(\boldsymbol{\xi}) \end{bmatrix} \mathbf{x}_k \;=\; \sum_{k=1}^{n} \mathbf{N}_k^e(\boldsymbol{\xi})\mathbf{x}_k \tag{27}$$

where n is the number of nodes in the element and $\mathbf{x}_k$ is the global coordinate of node k. The element displacements $\hat{\mathbf{u}}^e(\boldsymbol{\xi})$ in the local coordinate system are approximated using the same shape functions $\mathbf{N}_k^e(\boldsymbol{\xi})$:

$$\hat{\mathbf{u}}^e(\boldsymbol{\xi}) \;\simeq\; \sum_{k=1}^{n} \mathbf{N}_k^e(\boldsymbol{\xi})\underline{\hat{\mathbf{u}}}_k^e \;=\; \mathbf{N}^e(\boldsymbol{\xi})\underline{\hat{\mathbf{u}}}^e \tag{28}$$

where $\underline{\hat{\mathbf{u}}}^e = [\underline{\hat{\mathbf{u}}}_1^e; \underline{\hat{\mathbf{u}}}_2^e; \ldots; \underline{\hat{\mathbf{u}}}_n^e]$ is a column vector containing the nodal values of $\hat{\mathbf{u}}^e(\boldsymbol{\xi})$, and $\mathbf{N}^e(\boldsymbol{\xi}) = [\mathbf{N}_1^e(\boldsymbol{\xi}), \mathbf{N}_2^e(\boldsymbol{\xi}), \ldots, \mathbf{N}_n^e(\boldsymbol{\xi})]$. Likewise, the vector function $\boldsymbol{\chi}(\boldsymbol{\xi},\mathbf{x}_0)$ is approximated as:

$$\boldsymbol{\chi}(\boldsymbol{\xi},\mathbf{x}_0) \;\simeq\; \sum_{k=1}^{n} \mathbf{N}_k^e(\boldsymbol{\xi})\boldsymbol{\chi}_k \tag{29}$$

Its gradient $\nabla\boldsymbol{\chi}(\boldsymbol{\xi},\mathbf{x}_0)$ is a second-order tensor:

$$\nabla\boldsymbol{\chi}(\boldsymbol{\xi},\mathbf{x}_0) \;\simeq\; \sum_{k=1}^{n} \boldsymbol{\chi}_k \otimes \nabla N_k^e(\boldsymbol{\xi}) \tag{30}$$

which involves derivatives of the shape functions $N_k^e(\boldsymbol{\xi})$ with respect to the global coordinates $\mathbf{x}$. These are computed using the Jacobian matrix $\mathbf{J}^e$:

$$\nabla N_k^e(\boldsymbol{\xi}) \;=\; \mathbf{J}^{e-1}\nabla_\xi N_k^e(\boldsymbol{\xi}) \tag{31}$$

where ∇_ξ denotes the gradient operator with respect to $\boldsymbol{\xi}$. The volume integrals over V^e in equation (26) are subsequently transformed to the local coordinate $\boldsymbol{\xi}$ as:

$$\delta\hat{\mathbf{a}}(\mathbf{x}_0) \;\simeq\; \sum_{e=1}^{n^e} G \int_{-1}^{+1}\int_{-1}^{+1}\int_{-1}^{+1} \rho^e \nabla\boldsymbol{\chi}(\boldsymbol{\xi},\mathbf{x}_0)\cdot\hat{\mathbf{u}}^e(\boldsymbol{\xi})\det(\mathbf{J}^e)\,\mathrm{d}\xi_1\,\mathrm{d}\xi_2\,\mathrm{d}\xi_3 \tag{32}$$

Substituting the approximations (28) and (30), and separating $\underline{\hat{\mathbf{u}}}^e$ gives:

$$\begin{aligned} \delta\hat{\mathbf{a}}(\mathbf{x}_0) \;&\simeq\; \sum_{e=1}^{n^e} \left[G \int_{-1}^{+1}\int_{-1}^{+1}\int_{-1}^{+1} \rho^e \left(\sum_{k=1}^{n} \boldsymbol{\chi}_k \otimes \nabla N_k^e(\boldsymbol{\xi}) \right) \cdot \mathbf{N}^e(\boldsymbol{\xi}) \det(\mathbf{J}^e)\,\mathrm{d}\xi_1\,\mathrm{d}\xi_2\,\mathrm{d}\xi_3 \right] \underline{\hat{\mathbf{u}}}^e \\ &=\; \sum_{e=1}^{n^e} \mathbf{A}^e\underline{\hat{\mathbf{u}}}^e \end{aligned} \tag{33}$$

The $3 \times 3n$ matrix $\mathbf{A}^e$ yields the contribution of the nodal displacements $\underline{\hat{\mathbf{u}}}^e$ of element e to the total NN. The element matrices $\mathbf{A}^e$ are assembled into a global $3 \times 3N$ matrix $\mathbf{A}$, where N is the number of nodes inside the discretized volume V, yielding:

$$\delta\hat{\mathbf{a}}(\mathbf{x}_0) = \mathbf{A}\underline{\hat{\mathbf{u}}} \tag{34}$$

The vector $\underline{\hat{\mathbf{u}}}$ contains the nodal displacements inside V. The matrix $\mathbf{A}$ needs to be computed only once for a particular discretization, as it is independent of the displacement field $\hat{\mathbf{u}}(\mathbf{x})$. Hence, computing NN for any seismic displacement field becomes a simple post-processing step.

4 RESULTS

In this section, the Newtonian noise due to a plane P-wave with direction $\mathbf{e}_k = (\frac{1}{\sqrt{2}}, \frac{1}{\sqrt{2}}, 0)$ and unit amplitude is computed. The volume V consists of a homogeneous fullspace with a cavity with radius $r_0 = 20\,\mathrm{m}$ at $\mathbf{x}_0 = (0, 0, 0)$. The soil is modeled as a linear elastic medium with shear wave velocity $C_\mathrm{s} = 500\,\mathrm{m/s}$, dilatational wave velocity $C_\mathrm{p} = 1000\,\mathrm{m/s}$ and density $\rho = 1800\,\mathrm{kg/m^3}$.

4.1 Analytical solution

Analytical expressions for the NN induced by plane, harmonic waves propagating in a homogeneous fullspace with density ρ are first presented in order to validate the results obtained with our numerical model.

The soil displacements $\hat{\mathbf{u}}_\mathrm{p}(\mathbf{x})$ due to a plane P-wave with unit amplitude propagating in the direction $\mathbf{e}_\mathrm{k}$ (normalized) with wavenumber $k_\mathrm{p} = \omega/C_\mathrm{p}$ are equal to:

$$\hat{\mathbf{u}}_\mathrm{p}(\mathbf{x}) \;=\; \exp(-\mathrm{i}k_\mathrm{p}\mathbf{e}_\mathrm{k} \cdot \mathbf{x})\mathbf{e}_\mathrm{k} \tag{35}$$

Inserting equation (35) into equation (12) and evaluating the volume integral in spherical coordinates between radii r_0 and R yields the analytical expression for the NN at $\mathbf{x}_0$ [3]:

$$\delta\hat{\mathbf{a}}_\mathrm{p}(\mathbf{x}_0) \;=\; 8\pi\rho_1 G \left(\frac{j_1(k_\mathrm{p}r_0)}{k_\mathrm{p}r_0} - \frac{j_1(k_\mathrm{p}R)}{k_\mathrm{p}R} \right) \hat{\mathbf{u}}_\mathrm{p}(\mathbf{x}_0) \tag{36}$$

where $j_l(x)$ is the spherical Bessel function of the first kind and order l. Wave scattering by the cavity is not taken into account in this analytical solution. Assuming a fullspace, we take the limit for $R \to +\infty$, yielding:

$$\delta\hat{\mathbf{a}}_\mathrm{p}(\mathbf{x}_0) \;=\; 8\pi\rho_1 G \frac{j_1(k_\mathrm{p}r_0)}{k_\mathrm{p}r_0} \hat{\mathbf{u}}_\mathrm{p}(\mathbf{x}_0) \tag{37}$$

Note that the NN only depends on the displacement $\hat{\mathbf{u}}_\mathrm{p}(\mathbf{x}_0)$ at the position $\mathbf{x}_0$ of the mirror.

4.2 Influence of the domain size

We now consider an FE mesh of a cuboid soil volume V around the cavity with sides equal to $2R$ (figure 3a) consisting of at least 4 20-node solid elements per wavelength λ_p. The domain size R needs to be sufficiently large to reach convergence of the volume integral (12). To this end, we compare numerical predictions on a grid with increasing ratio R/λ_p with the

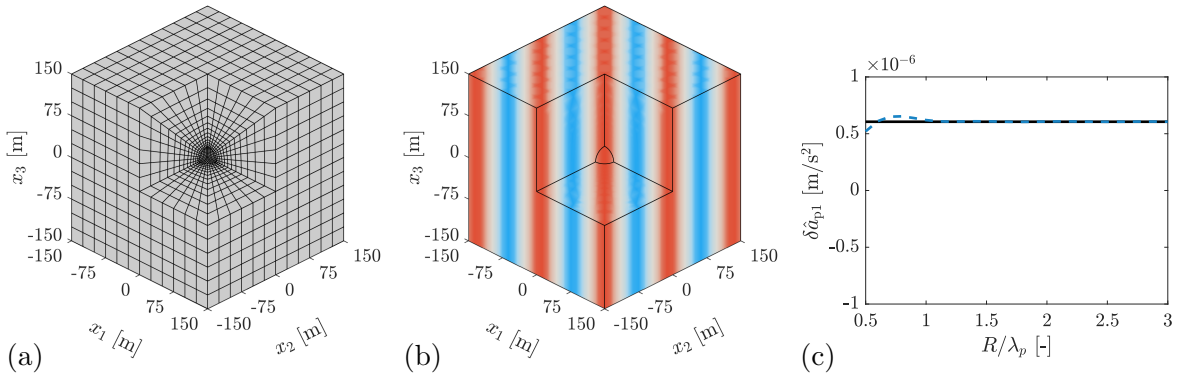

Figure 3: (a) FE mesh and (b) soil displacements $\hat{u}_{\mathrm{p1}}(\mathbf{x})$ for $R/\lambda_{\mathrm{p}} = 1.5$. (c) Newtonian noise $\delta\hat{a}_{\mathrm{p1}}(\mathbf{x}_0)$ as a function of R/λ_{p} computed analytically (——) and with the numerical model (- - -).

analytical solution for a fullspace given by equation (37). The wavelength $\lambda_{\mathrm{p}} = 100\,\mathrm{m}$ is fixed, corresponding to an excitation frequency of 10 Hz.

Figure 3a shows the FE mesh for $R/\lambda_{\mathrm{p}} = 1.5$. The mesh is denser close to the cavity to accurately capture the strongly decaying function $\boldsymbol{\chi}(\mathbf{x}, \mathbf{x}_0)$. The soil displacements $\hat{u}_{\mathrm{p1}}(\mathbf{x})$ due to the P-wave are shown in figure 3b. For now, we disregard wave scattering by the cavity. Figure 3c shows the NN $\delta\hat{a}_{\mathrm{p1}}(\mathbf{x}_0)$. As the domain size R increases, the numerical result approaches the analytical solution for the fullspace. Convergence is reached for a domain size $R \simeq 1.5\lambda_{\mathrm{p}}$, which is used in the following.

4.3 Influence of the cavity radius and wave scattering

We now take into account wave scattering by the cavity and consider three cavity radii equal to 10 m, 20 m and 40 m. The FE mesh consists of the inner volume V_{i}, the outer volume V_{e} and the PML (figure 4). For the computation of the scattered wave field $\hat{\mathbf{u}}^{\mathrm{sc}}(\mathbf{x})$, a hysteretic loss factor of 0.02 is assumed.

Figure 5 shows the incoming wave field $\hat{u}_1^{\mathrm{inc}}(\mathbf{x})$, the scattered wave field $\hat{u}_1^{\mathrm{sc}}(\mathbf{x})$ and the total wave field $\hat{u}_1(\mathbf{x})$ for $\lambda_{\mathrm{p}} = 100\,\mathrm{m}$ (10 Hz) and $r_0 = 20\,\mathrm{m}$. The amplitude of the scattered wave

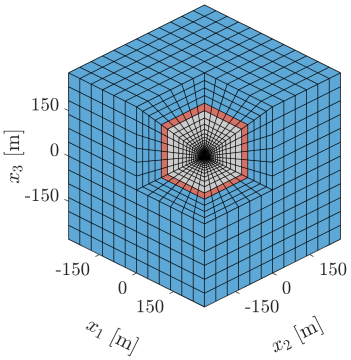

Figure 4: FE mesh used for the computation of the scattered wave field $\hat{\mathbf{u}}^{\mathrm{sc}}(\mathbf{x})$ due to an incoming P-wave with wavelength $\lambda_{\mathrm{p}} = 100\,\mathrm{m}$ (10 Hz) impinging on a cavity with $r_0 = 20\,\mathrm{m}$. The mesh consists of the volume V_{i} (gray), V_{e} (red) and the PML (blue) (cfr. figure 2a).

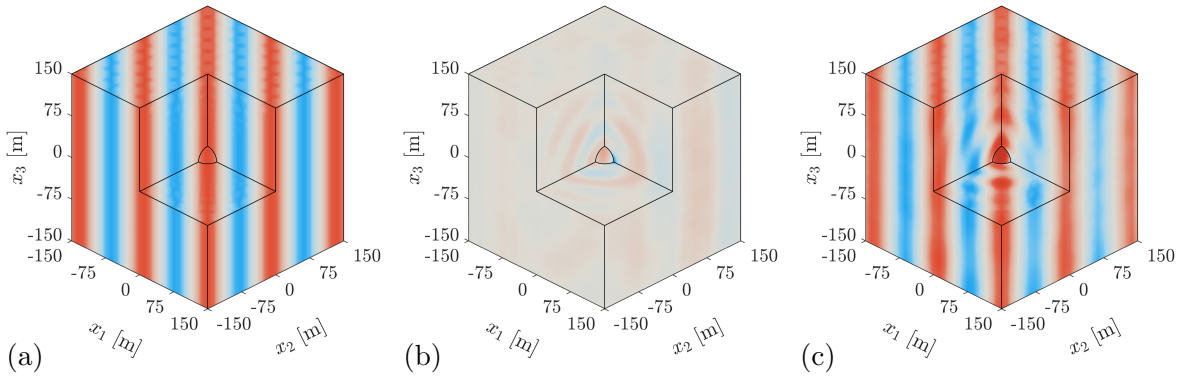

Figure 5: (a) Incoming wave field $\hat{u}_1^{\text{inc}}(\mathbf{x})$, (b) scattered wave field $\hat{u}_1^{\text{sc}}(\mathbf{x})$ and (c) total wave field $\hat{u}_1(\mathbf{x})$ for a P-wave with wavelength $\lambda_{\text{p}} = 100\,\text{m}$ (10 Hz) impinging on a cavity with $r_0 = 20\,\text{m}$.

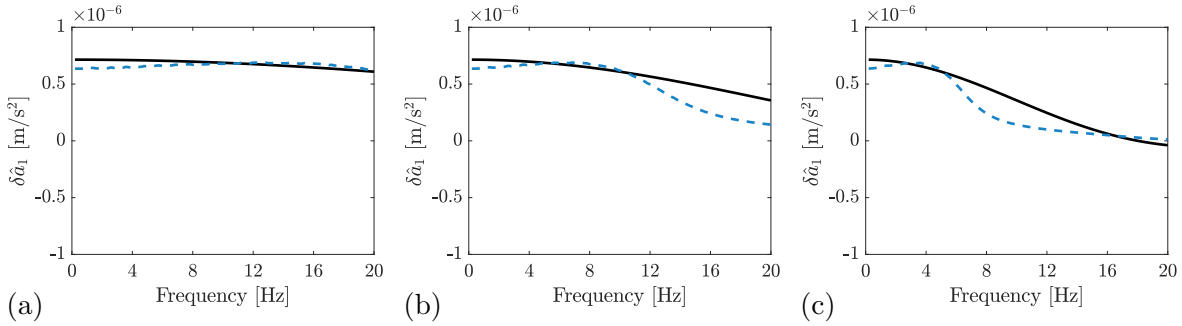

Figure 6: Newtonian noise $\delta\hat{a}_1(\mathbf{x}_0)$ as a function of frequency computed on a domain with $R = 1.5\lambda_{\text{p}}$ and cavity radius (a) $r_0 = 10\,\text{m}$, (b) $r_0 = 20\,\text{m}$ and (c) $r_0 = 40\,\text{m}$. Results are computed with (- - -) and without (——) wave scattering by the cavity.

field $\hat{u}_1^{\text{sc}}(\mathbf{x})$ is much smaller than the amplitude of the incoming wave field $\hat{u}_1^{\text{inc}}(\mathbf{x})$.

Figure 6b shows the NN $\delta\hat{a}_1(\mathbf{x}_0)$ for the fullspace with cavity radius $r_0 = 20\,\text{m}$. The result without taking into account wave scattering is shown as a reference. At low frequencies, where the wavelength λ_{p} is large compared to the radius r_0, the effect of wave scattering on the NN is limited. Above 12 Hz, where $\lambda_{\text{p}} \simeq 4r_0$, the predicted NN is lower compared to the reference solution without wave scattering.

Figure 6a shows that, for a smaller cavity radius $r_0 = 10\,\text{m}$, the NN at low frequencies remains approximately the same, while the NN at high frequencies is higher. The effect of wave scattering is also not very important for the considered soil characteristics. For a larger cavity radius $r_0 = 40\,\text{m}$ (figure 6c), however, the NN clearly decreases with increasing frequency. A significant discrepancy between the results with and without wave scattering is observed between 6 Hz ($\lambda_{\text{p}} \simeq 4r_0$) and 16 Hz ($\lambda_{\text{p}} \simeq 1.5r_0$). When the wavelength λ_{p} approaches the cavity radius r_0, the strongly scattered wave field results in a (on average) zero contribution to the NN.

5 CONCLUSIONS

This paper presents a numerical model to predict NN due to seismic wave propagation in the soil. Gaussian quadrature on an FE mesh is used to numerically evaluate the volume integrals

governing NN. Any soil heterogeneity and cavity shape can be meshed. A subdomain formulation is also suggested to take into account wave scattering by the cavity. The model is validated for a spherical cavity inside a homogeneous fullspace, for which analytical expressions for the NN are available. It is concluded that the NN reduces with increasing cavity radius r_0, except at low frequencies, where the wavelength in the soil is much larger than the cavity. We also show that the influence of wave scattering by the cavity can be important for wavelengths between $1.5r_0$ and $4r_0$, resulting in lower NN for the considered soil characteristics.

ACKNOWLEDGEMENTS

Results presented in this paper have been obtained within the frame of the FWO-IRI project "Essential Technologies for the Einstein Telescope". The financial support of the Research Foundation Flanders (FWO) is gratefully acknowledged.

REFERENCES

[1] F. Amann et al. Site-selection criteria for the Einstein Telescope. *Review of Scientific Instruments*, 91:094504, 2020.

[2] J.C. Driggers, J. Harms, and R.X. Adhikari. Subtraction of Newtonian noise using optimized sensor arrays. *Physical Review D*, 86:102001, 2012.

[3] J. Harms. Terrestrial gravity fluctuations. *Living Reviews in Relativity*, 22:6, 2019.

[4] E. Kausel and J.M. Roësset. Stiffness matrices for layered soils. *Bulletin of the Seismological Society of America*, 71(6):1743–1761, 1981.

[5] J. Bielak, K. Loukakis, Y. Hisada, and C. Yoshimura. Domain reduction method for three-dimensional earthquake modeling in localized regions, Part I: Theory. *Bulletin of the Seismological Society of America*, 93(2):817–824, 2003.

[6] J.P. Bérenger. A perfectly matched layer for the absorption of electromagnetic waves. *Journal of Computational Physics*, 41:115–135, 1994.

[7] U. Basu and A.K. Chopra. Perfectly matched layers for time-harmonic elastodynamics of unbounded domains: theory and finite-element implementation. *Computer Methods in Applied Mechanics and Engineering*, 192(11-12):1337–1375, 2003.